Smelting of Pyrolyzed Lithium-Ion Battery Black Mass using a Calcium-Aluminate Slag System

Marcus Sommerfeld, Gunnar Hovestadt, Prof. Dr. Ing. Dr. h.c. Bernd Friedrich

IME Process Metallurgy and Metal Recycling, Institute of RWTH Aachen University
Intzestraße 3
52056 Aachen, Germany

Abstract

Keywords: Pyrometallurgy, lithium-ion battery recycling, thermochemical modelling, lithium slag

The ongoing trend of vehicle electrification and the increasing demand for battery-powered consumer electronic devices led to a huge demand for raw materials for the manufacturing of batteries with a high energy density. Especially the demand for cobalt, nickel and lithium is increasing due to the demand for the battery industry. Especially for a country with no sufficient primary resources, the recycling of spent lithium-ion batteries (LIBs) represents a potential source of raw materials whose valuable metal-rich components are currently only insufficiently recovered. This paper explores the options of smelting pyrolyzed lithium-ion battery black mass in a laboratory-scale electric arc furnace. Due to the high graphite content in the black mass, a smelting would result in a slag-graphite mixture, which is unsuitable for a smelting process. This paper investigates the option, to use graphite as a reducing agent for copper(II)-oxide during a pyrometallurgical smelting process. An alloy containing copper, cobalt, nickel and iron is produced in the furnace. Burnt lime is added as a flux and therefore the slag can be assigned to the calcium-aluminate slag system. A thermochemical simulation study is carried out to aid the experimental smelting trials. The remaining content of lithium in the slag is assayed by ICP-OES to determine the volatilization behavior of lithium for various additions of burnt lime. An analysis of the slag by x-ray diffraction is carried out to determine the main mineral phases of the slag.

By adding lime and smelting at 1800 °C, it was possible to volatilize 80.4 % of lithium from the raw material. The lithium content of the slag was still 2.55 wt% in the best case. The lowest contents of nickel, cobalt and copper in the slag were 71 ppm, 0.06 wt% and 0.28 wt% respectively in the best case.

1 Introduction and State of the Art

Lithium-ion batteries (LIBs) are an important energy storage system and already used in a wide range of applications, especially in portable devices [1–7]. In addition to portable applications, LIBs are also used as an intermediate energy storage in stationary applications to stabilize decentralized power systems [2–5, 8, 9]. Since the applications for LIBs are currently increasing, a considerable higher demand for strategic or critical resources like lithium, cobalt and nickel can be expected shortly. Currently, those elements are mostly obtained from primary sources [2]. To cover the increasing demand for those elements, efficient recycling is unavoidable in addition to an expansion of mining capacities [5]. Research regarding the recycling of spent LIBs has been carried out investigating single or combined processes based on mechanical, pyrometallurgical, hydrometallurgical and pyrolysis processes [5, 9–33]. In this article, a pyrometallurgical process in a laboratory-scale electric arc furnace is investigated. The pyrometallurgical process in an electric arc furnace has the advantage, that it can tolerate a variable composition of feed material or that it is adaptable to newer battery generations. Furthermore, the throughputs in a high-temperature plant can be considered higher compared to hydrometallurgical operations. However, due to the high temperatures needed in the process, pyrometallurgical operations are energy-intensive. Also, it is still not clear how lithium should be recovered in the best way.

The investigated material in this article is black mass obtained by dismantling of end-of-life batteries, pyrolysis and further comminution and separation of the coarse metallic fraction. The same material was already investigated using a SiO_2-Al_2O_3-Li_2O slag system to study the enrichment of lithium in the slag [22] in a pyrometallurgical process. In comparison to the previous work, this study aims to volatilize lithium and therefore enrich it in the flue dust. While elements like cobalt, nickel and copper are normally enriched in a metal phase during pyrometallurgical treatment of battery scrap [18, 22, 24, 26, 29, 34–39], lithium is either enriched in the slag [22, 35, 37] or the flue dust [24, 26, 36, 38].

Studies regarding the recovery of lithium from slag [40–43] were already investigated in the past. Fewer studies were found for the recovery of lithium from flue dust. Georgie-Maschler et.al. [24] reported for the generated flue dust, that leaching efficiencies over 90 % can be achieved using sulfuric acid and the obtained lithium carbonate has a purity higher than 99 wt%. The used flue dust was generated in a technical-scale electric arc furnace campaign and contained 20.1 wt% lithium, major impurities were calcium, cobalt and carbon with 22.3 wt%, 19.4 wt% and 13.2 wt% respectively [24]. Hu et.al. [36] investigated flue dust generated in a Tamman furnace trial with X-ray diffraction, the flue dust mostly contained Li_2CO_3 and LiF [36]. However, it can be expected, that the static conditions in a resistance heated furnace lead to less material losses and flue dust in general compared to an industrial furnace and therefore to purer flue dust. Hu et.al. [39] also carried out pilot-scale experiments in an electrical arc furnace, were the flue dust contained impurities. Those samples contained 12.40 wt% and 13.02 wt% lithium and were treated by carbonated-water leaching. Obtained salt samples contained up to 18.0 wt% lithium [39].

Even though little research is available regarding the recovery of lithium from flue dust generated during smelting of spent LIBs, it is postulated, that the recovery from flue dust is easier compared to the recovery from slag [36, 38].

2 Experimental Details

The black mass investigated in this work was provided by Accurec Recycling GmbH. End-of-life batteries were manually dismantled to remove copper cables, steel casings, electric components and plastics. Afterward, the active mass was pyrolyzed to deactivate the dismantled batteries and to evaporate the electrolyte. The pyrolyzed active mass was furthermore treated by comminution and sieving to separate a coarse fraction rich in iron, copper and aluminum, the fine black mass fraction was then pelletized for the smelting trials. The black mass was analyzed by:

- Inductively coupled plasma-optical emission spectrometry (ICP) (Spectro CIROS Vision, Spectro Analytical Instruments GmbH, Kleve Germany), two measurements per sample
- Carbon analysis with a combustion method (ELTRA CS 2000, ELTRA GmbH, Haan, Germany), three measurements per sample
- Fluorine analysis with ion chromatography (IC) (881 Compact IC pro, Deutsche Metrohm GmbH & Co. KG, Filderstadt, Germany), two measurements per sample

The composition of the black mass used for the trials and the following FactSage™ [44] simulation is shown in Table 1. Noteworthy is the high cobalt content in the sample compared to the manganese and nickel content. Increasing nickel and manganese contents can be expected in the future in end-of-life batteries compared to the investigated black mass used in this work, because nickel and manganese are used nowadays in batteries to replace cobalt [45].

Table 1: Composition of the black mass in wt%

Element	**Co**	**Fe**	**Mn**	**Al**	**Cu**	**Si**	**Zn**	**Ni**	**Ag**	**Li**	**C**	**F**
wt%	22.0	6.51	0.75	3.88	4.69	0.37	0.11	2.71	0.32	2.24	20.5	2.5

Furthermore, copper(II)-oxide (Lomberg GmbH, Oberhausen, Germany) was used in this work as an oxidizing agent with a CuO-content above 98.9 wt%. Burnt lime (Rheinkalk GmbH, Wülfrath, Germany) was used as a flux with a CaO-content of 94.6 wt%. The composition of those two raw materials were assumed to be 100 wt% of CuO and CaO respectively for calculations and simulations.

The smelting trials were carried out in a direct-current electric arc furnace. Figure 1 shows a schematic diagram of the furnace and a picture of the tapping operation after a trial. The electrical current of the furnace is between zero and thousand amperes and the voltage between zero and eighty volts. The power is variable. As the voltage is dependent on the electrical resistivity of the furnace components and the charged material, the electrical current is adjusted by the operating system to obtain the desired power. The position of the graphite electrode can be adjusted with a hydraulic system.

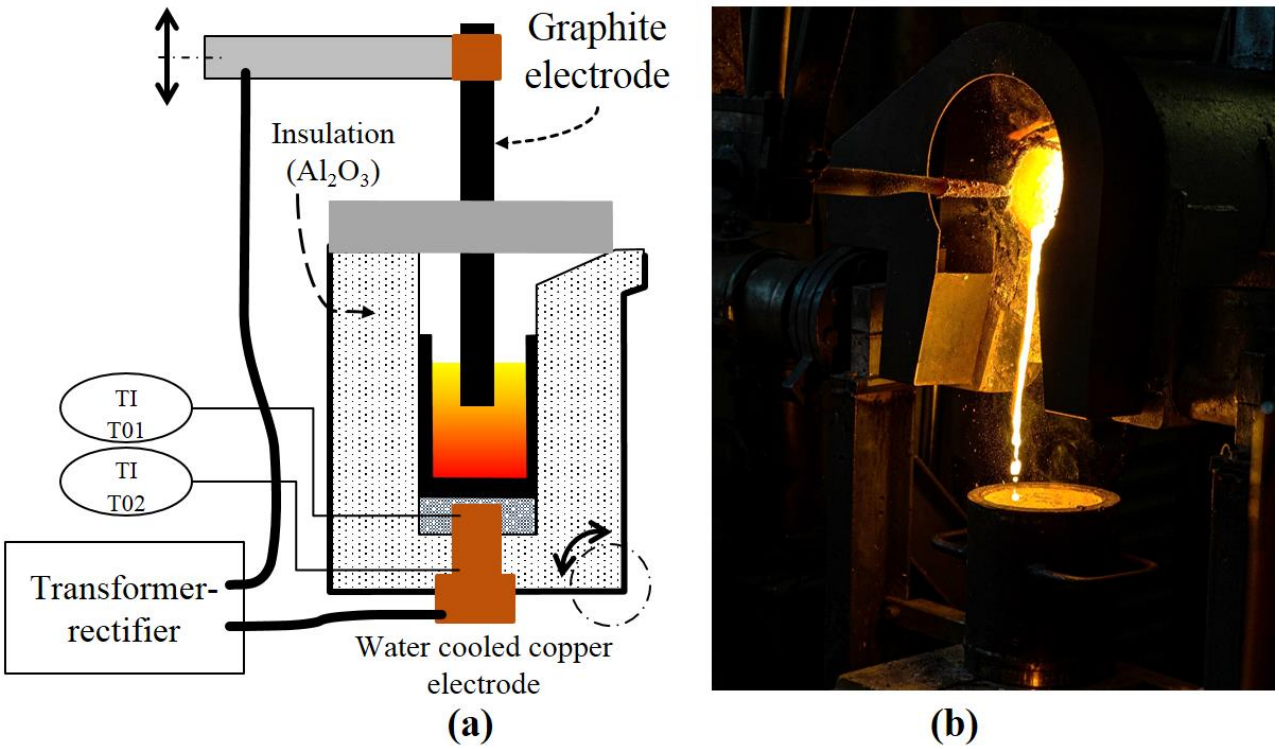

Figure 1: Laboratory electric arc furnace **(a**) schematic diagram **(b)** tapping of the furnace

The crucible used for the smelting was a high-purity graphite crucible with a volume of 2 L. The inner diameter of the crucible was 120 mm. The graphite electrode used had a diameter of 30 mm and was immersed in the slag during smelting. Before the trial, the crucible was pre-heated to roughly 1000 °C. Charging of pelletized electrode mass, copper(II)-oxide and lime was done simultaneously using a small shovel. In total, 3500 g of pelletized black mass was fed per trial. The lime addition was varied to investigate the influence of lime on the process. The copper(II)-oxide addition per trial was between 3500 g and 4725 g and was adjusted based on the amount of graphite still present on the slag. The variation can be explained by the fact, that the copper(II)-oxide does not only react with the graphite in the black mass, but also with the graphite crucible or graphite electrode. Furthermore, copper(II)-oxide can be reduced with carbon monoxide [46], present in the ascending gases. Therefore, the amount of copper(II)-oxide reacting with graphite from the black mass vary, if other graphite or carbon monoxide sources react with the copper(II)-oxide. The charging of material took roughly 120 minutes per trial and after the material was charged, a holding time of 20 minutes was carried out. The temperature was a variable parameter in this work, trials were carried out either at 1700 °C or 1800 °C, the temperature was measured discontinuously using type B thermocouple immersion probes (Heraeus Electro-Nite GmbH & Co. KG, Hagen, Germany). The accuracy is estimated to be ±25 °C. After the holding time, the melt was poured from the crucible into a cast-iron mould. Slag samples were taken from the bulk slag phase after solidification and were analyzed.

3 Evaluation of the Smelting Trials

Twelve trials were carried out in total, the temperature and the lime addition were varied. Two trials were carried out per parameter. The lime-additions investigated were 7 wt%, 10 wt% and 13 wt% in relation to the black mass pellets. The investigated slag temperatures were 1700 °C and 1800 °C. Table 2 shows the mean chemical composition of the slag samples generated in the trials. The same analytical equipment used for the black mass was used for the slag samples. In addition, the slags were also analyzed by wavelength dispersive x-ray fluorescence (XRF) spectroscopy as fused cast beats (Axios^{mAX}, Malvern Panalytical B.V., Almelo, Netherlands) using the wide range oxide (WROXI) calibration. Carbon and sulfur analysis was also carried out, but is not presented in the table, as the results were insignificant. The carbon content in the slag was between 0.13 wt% and 0.55 wt% and the sulfur content was between 0.16 wt% and 0.18 wt%.

Table 2: Mean chemical composition of slag samples

		Mean Composition									
Temperature in °C	**Lime-addition in wt%**	**Li**	**Ni**	**Co**	**Cu**	**F**	**Al_2O_3**	**CaO**	**Mn**	**Fe**	**SiO_2**
			ICP			**IC**			**XRF**		
		wt%	**ppm**	**wt%**	**wt%**	**wt%**	**wt%**	**wt%**	**wt%**	**wt%**	**wt%**
1700	7	6.20	183	0.13	0.67	2.07	34.00	33.15	0.95	0.33	2.29
	10	5.68	341	0.22	0.87	2.18	33.45	34.85	0.61	0.34	2.30
	13	4.49	339	0.23	0.68	1.75	28.30	44.55	0.60	0.44	2.07
1800	7	5.56	293	0.21	0.64	1.91	37.05	34.10	0.42	0.28	2.58
	10	4.23	209	0.13	0.46	1.51	33.60	42.10	0.14	0.13	2.48
	13	2.55	71	0.06	0.28	1.30	32.60	47.11	0.08	0.09	2.80

Metal samples were not analyzed, since the concentration of valuable metals like nickel, cobalt and copper is already relatively low in the slag. Furthermore, it is difficult to sample the metal alloy, since two immiscible phases occurred, one rich in copper and one rich in cobalt. This was also observed in a previous paper and further analyzed [22].

3.1 Behaviour of Lithium during Smelting

As flue dust and gas were not sampled after or during the trials, the volatilization is not directly analyzed. Instead, the fraction of lithium distributed into the slag phase is evaluated. Figure 2 shows the lithium slagging in relation to the addition of lime for two temperatures. As two trials were carried out per parameter, error bars indicate the deviation from the mean results. A comparison with a FactSage^{TM} model using a closed system is also shown in the Figure. The losses of lithium into the metal alloy are also not evaluated in this article. This simplification was made, because the amount of lithium transferred to the metal is relatively small compared to the lithium volatilized or present in the slag. In previous trials, only 2.8 % of the lithium from the input material was present in the metal alloy afterward [22].

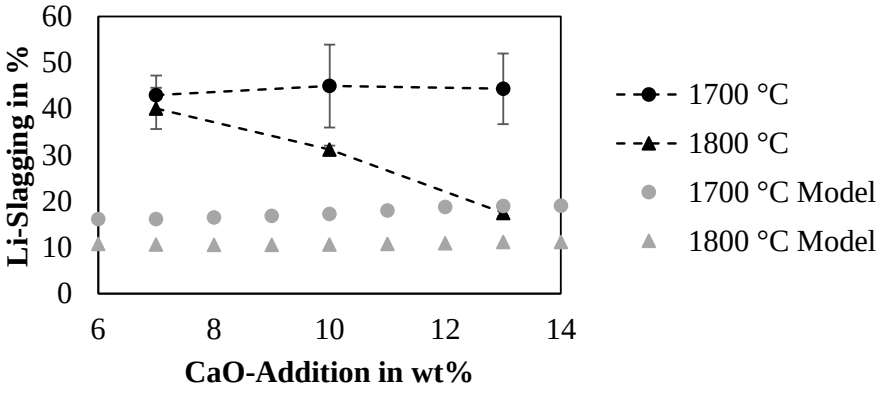

Figure 2: Influence of lime addition on the lithium slagging

In all trials, the lithium losses to the slag were higher compared to the FactSage™ model, furthermore the lime addition does not improve the lithium volatilization according to the model, instead, slightly higher lime additions even increase the lithium slagging. In the trials at 1700 °C, lime did not affect the lithium volatilization. The mean values for the lithium slagging are between 42.95 % and 44.93 % at 1700 °C. At 1800 °C, the effect of lime on the lithium slagging is more obvious. Adding 7 wt% lime still leads to a lithium slagging of 40.07 %. Increasing the lime addition to 10 wt% and 13 wt% decreases the lithium slagging to 31.16 % and 17.45 % respectively, which is still higher compared to the model. Also, the positive influence of the lime addition on the lithium volatilization was not predicted by the model.

As added lime is sometimes directly consumed by the off-gas suction of the furnace, the CaO-concentration in the slag was also compared with the lithium concentration in Figure 3. This was carried out for the trials carried out at 1700 °C and 1800 °C and compared with the FactSage™ model assuming a closed system.

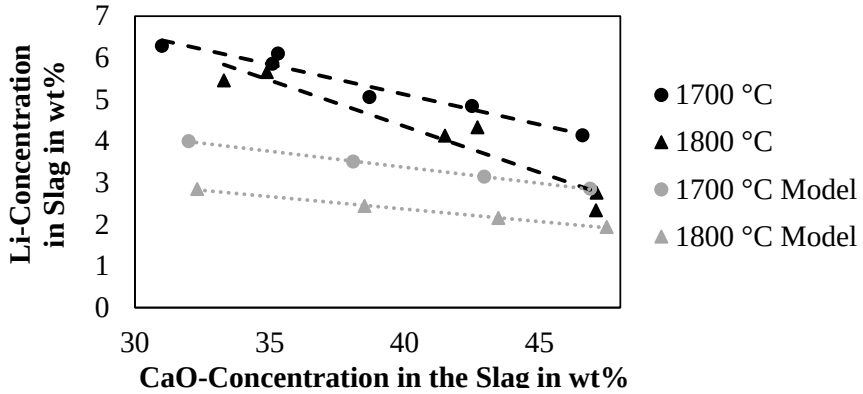

Figure 3: Lithium concentration in the slag compared to the concentration of CaO

Lithium concentrations between 6.29 wt% and 2.34 wt% were observed in the slag. In all cases, the lithium concentration was higher than the predictions by the model, but higher concentrations of CaO in the slag lead to lower lithium concentrations in the end. Of course, this is also explainable by further dilution of lithium by added lime. To describe the relationship between the lithium concentration and CaO-concentration linear equations in the form of Equation 1 were compiled.

$$wt\%_{Li} = m \cdot wt\%_{CaO} + b \quad (1)$$

Table 3 lists the slope (m), vertical axis intercept (b) and the coefficient of determination (R^2).

Table 3: Linear relations for the lithium concentration compared to the concentration of CaO

Graph	m	b	R^2
1700 °C	-0.1447	10.908	0.9495
1700 °C Model	-0.0769	6.4527	0.9995
1800 °C	-0.2211	13.202	0.9230
1800 °C Model	-0.0600	4.7736	0.9979

According to Table 3, the slope at 1800 °C is the most negative value and even at 1700 °C, the slope is more negative compared to the slopes of the FactSage™ model. Since the slope in the model is also negative, but the lithium slagging is slightly increasing with lime additions according to Figure 3, the negative slope for the model is probably due to dilution effects based on the lime addition and cannot be explained by enhanced volatilization. The more negative slope achieved during the trials is therefore explainable by increasing volatilization, if the CaO-content of the slag is increasing.

Another deviation from the FactSage™ model is the behavior of fluorine during smelting. Figure 4 shows the slagging of fluorine according to the FactSage™ model and from the experiments for different lime additions and temperatures. With increasing lime additions, the slagging of fluorine should increase as well according to the model, this was not confirmed by experiments, especially for 1800 °C the slagging of fluorine is decreasing with increasing lime additions. Furthermore Figure 4 shows the relationship between the slagging of fluorine and the slagging of lithium.

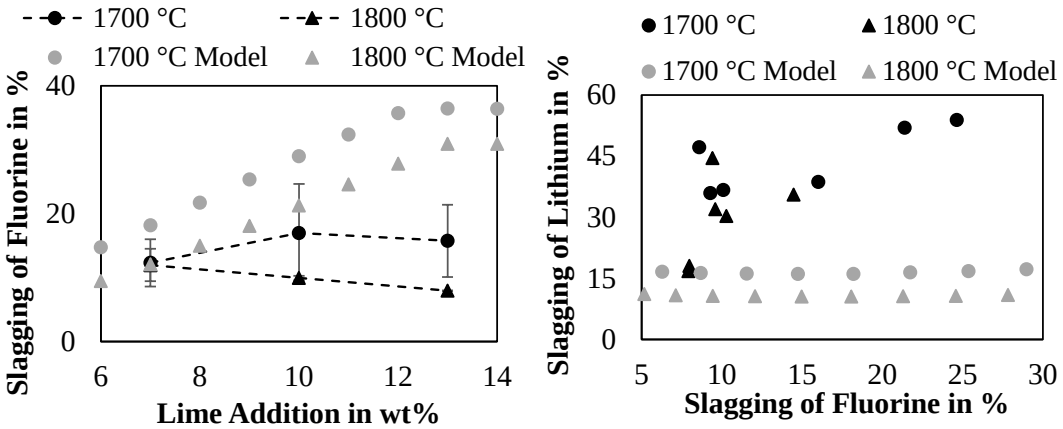

Figure 4: Slagging of fluorine compared to the lime addition and slagging of Lithium compared to the slagging of fluorine

As can be seen in Figure 4, the model shows only a slight impact of the fluorine slagging on the lithium slagging, however, in the trials a deviation can be seen. While eight trials showed a fluorine

slagging below 11 %, four trials were above 11 %. Interestingly, the two trials with the highest fluorine slagging lead to the highest lithium slagging. The two trials with the lowest fluorine slagging lead to the lowest lithium slagging and therefore resulted in the highest volatilization of fluorine and lithium. Based on those results, the vapor pressure of lithium fluoride was further examined using FactSage™. Figure 5 shows the vapor pressure of lithium compounds, that could be relevant for the volatilization of lithium during the investigated process.

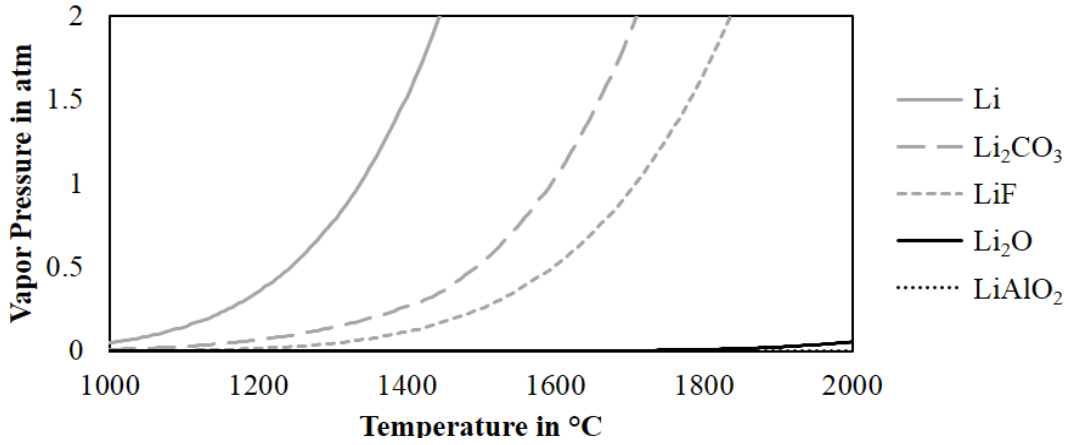

Figure 5: Vapor pressure of lithium compounds according to FactSage™

Metallic lithium has the highest vapor pressure, but due to the ignoble character of lithium, if metallic lithium would evaporate it would oxidize in the off-gas. Lithium carbonate is another compound, which has a relatively high vapor pressure at elevated temperatures. The presence of Li_2CO_3 in flue dust samples was also confirmed by Hu et.al. [36], who explained the presence of Li_2CO_3 by the reaction of metallic Lithium with oxygen and carbon monoxide in the off-gas. Hu et.al. [36] also confirmed the presence of lithium fluoride in their flue dust. According to Figure 5, lithium fluoride has a vapor pressure of one atm at 1700 °C and could therefore directly evaporate during all trials, assuming ideal behaviour. Maybe, the high slagging of lithium and fluorine shown in Figure 4 at 1700 °C, could be due to kinetic reasons, a longer holding time might enable further volatilization of lithium fluoride, which would decrease the slagging of lithium and fluorine. Furthermore, as Figure 5 only considers pure elements, the volatilization of lithium fluoride during the trials could be hindered due to lower activity coefficients. The vapor pressure of Li_2O and $LiAlO_2$ is relatively small compared to the other compounds and therefore direct volatilization of those compounds seems rather unlikely.

Based on the results presented in this subchapter, a clear deviation was observed between the experimental results and the FactSage™ simulation carried out to aid the experimental work. Especially the relationship between the slagging of lithium and fluorine compared to the addition of lime is an obvious deviation. Since FactSage™ only simulates the thermochemical equilibrium, kinetic reasons could be used to explain the higher slagging of lithium. However, this explanation is not suitable to explain the higher slagging of fluorine observed in the trials compared to the FactSage™ simulation. This implicates, that in future research the behaviour of lithium and fluorine has still to be investigated thoroughly, since the current databases might not yield reliable results in this situation.

3.2 Behaviour of Copper, Cobalt and Nickel during Smelting

Even though this article focuses on the volatilization of lithium, the aim of the investigated pyrometallurgical smelting operation is to enrich cobalt, nickel and copper in the metal phase. As the metal obtained in the trials was inhomogeneous and contained a copper-rich phase and a cobalt-rich phase, the measured concentration of those elements in the slag was used to evaluate the recovery. A possible method to recover cobalt, nickel and copper from the produced alloy could be a hydrometallurgical treatment as proposed by Keber et.al. [47]. As iron and manganese are considered as an impurity in this scenario, the concentration of cobalt, copper and nickel in the slag was compared with the manganese and iron concentration in the slag. Figure 6 shows the concentration of cobalt in the slag in relation to the iron and manganese concentration in the slag.

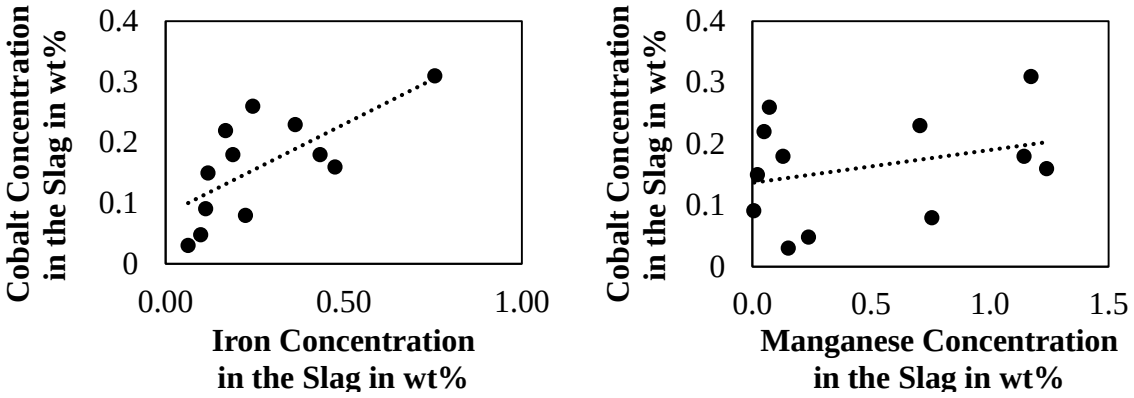

Figure 6: Cobalt concentration in the slag compared to the concentration of iron and manganese

The highest concentration of cobalt in the slag was 0.31 wt%, while the iron concentration was 0.76 wt% and the manganese concentration was 1.17 wt%. The lowest cobalt concentration observed was 0.03 wt%, however, to achieve this a considerable amount of manganese and iron has to be reduced as well. The mean cobalt concentration from twelve trials was 0.16 wt%.

The same evaluation was carried out for nickel and is shown in Figure 7.

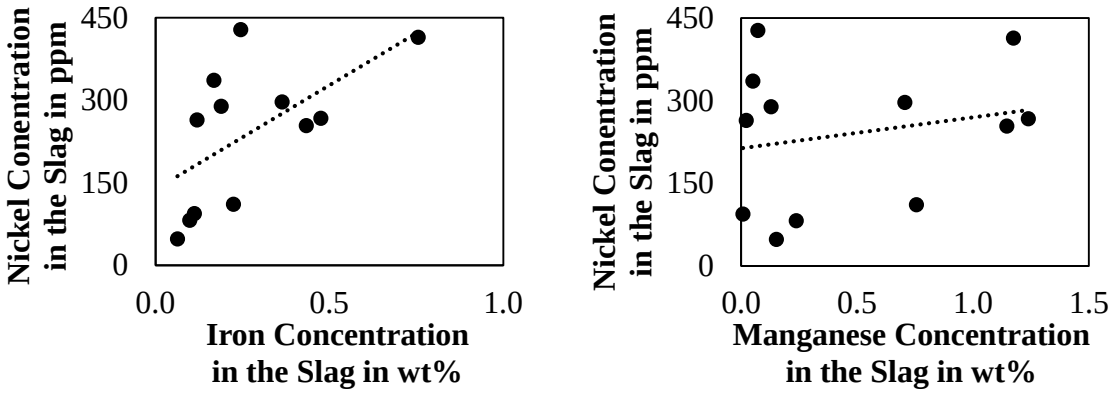

Figure 7: Nickel concentration in the slag compared to the concentration of iron and manganese

A similar trend compared to the cobalt concentration can be seen for nickel, as the lowest nickel concentrations were observed, if the iron concentrations are relatively low. However, the influence of the manganese concentration is less clear, because seven trials yielded a slag with a manganese concentration below 0.5 wt%, but three of those slags had a nickel concentration below 100 ppm, while the other four had a nickel concentration above 250 ppm and one of those samples even had the highest nickel concentration. The mean nickel concentration from twelve trials was 240 ppm.

Figure 8 shows the same evaluation for the copper concentration in the slag.

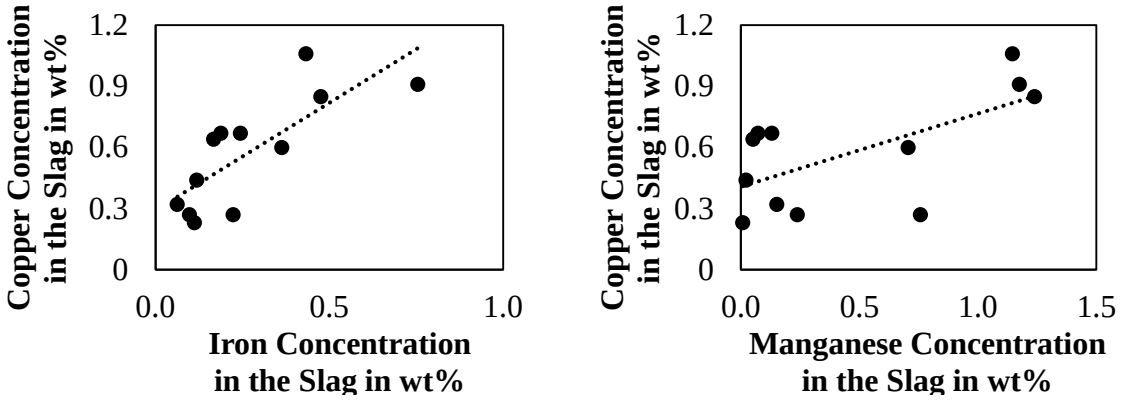

Figure 8: Copper concentration in the slag compared to the concentration of iron and manganese

The copper concentration in the slag is higher compared to cobalt and nickel, this could be due to the high amount of copper in the metal phase. Furthermore, the copper concentration in the slag is considerably higher, if the iron concentration is increased in the slag. The highest copper concentrations in the slag are observed for the three trials with the highest manganese concentration in the slag. Below a manganese concentration of 1 wt%, there is no general trend observable. The mean copper concentration from twelve trials was 0.58 wt%.

Selectively reducing cobalt, nickel and copper while leaving iron and manganese in the slag seems to be difficult, which was already observed for the SiO_2-Al_2O_3-Li_2O slag system [22]. Especially the relations for the concentration of valuable metals compared to the concentration of iron is relatively obvious, more residual iron in the slag leads to losses of valuable metals. For manganese the relation between the valuable metal content is less clear, however it is fair to say, that a high concentration of manganese leads to higher concentrations of valuable metals in the slag. Lower concentrations of manganese in the slag can lead to lower concentrations of valuable metals in the slag, but higher concentrations of valuable metals were also observed. But even in the case of higher valuable metal contents, the concentrations are still relatively low.

4 Mineralogical Slag Evaluation

To further investigate the slag a mineralogical characterization was carried out. Based on the results in chapter three, the slag still contains high lithium concentrations up to 6.20 wt%, other major components in the slag are aluminum and calcium. Therefore, binary Al_2O_3-CaO phase diagrams were

simulated with FactSage™ investigating different constant Li_2O-contents. In addition, the slag samples were investigated using X-ray diffraction (XRD).

4.1 CaO-Al_2O_3-(Li_2O) Phase Diagrams

Based on the measured compositions presented in Table 4, a mean normalized composition was calculated only considering the Al_2O_3-, CaO- and Li_2O-content of the slag, to compare these normalized compositions with the simulated phase diagrams, which only contain Al_2O_3, CaO and Li_2O.

Table 4: Mean normalized slag composition for the Al_2O_3-CaO-Li_2O system

Temperature in °C	Lime addition in wt%	Li_2O-content in wt%	Al_2O_3-content in wt%	CaO-content in wt%
	7	16.6	42.3	41.1
1700	10	14.8	39.0	46.2
	13	11.8	34.3	54.0
	7	14.4	44.6	41.0
1800	10	10.7	39.6	49.6
	13	6.4	38.3	55.3

The Li_2O-contents chosen for the binary phase diagrams presented are 5 wt%, 10 wt% and 15 wt%. Figure 9 shows the Al_2O_3-CaO phase diagram with a constant Li_2O-content of 5 wt%.

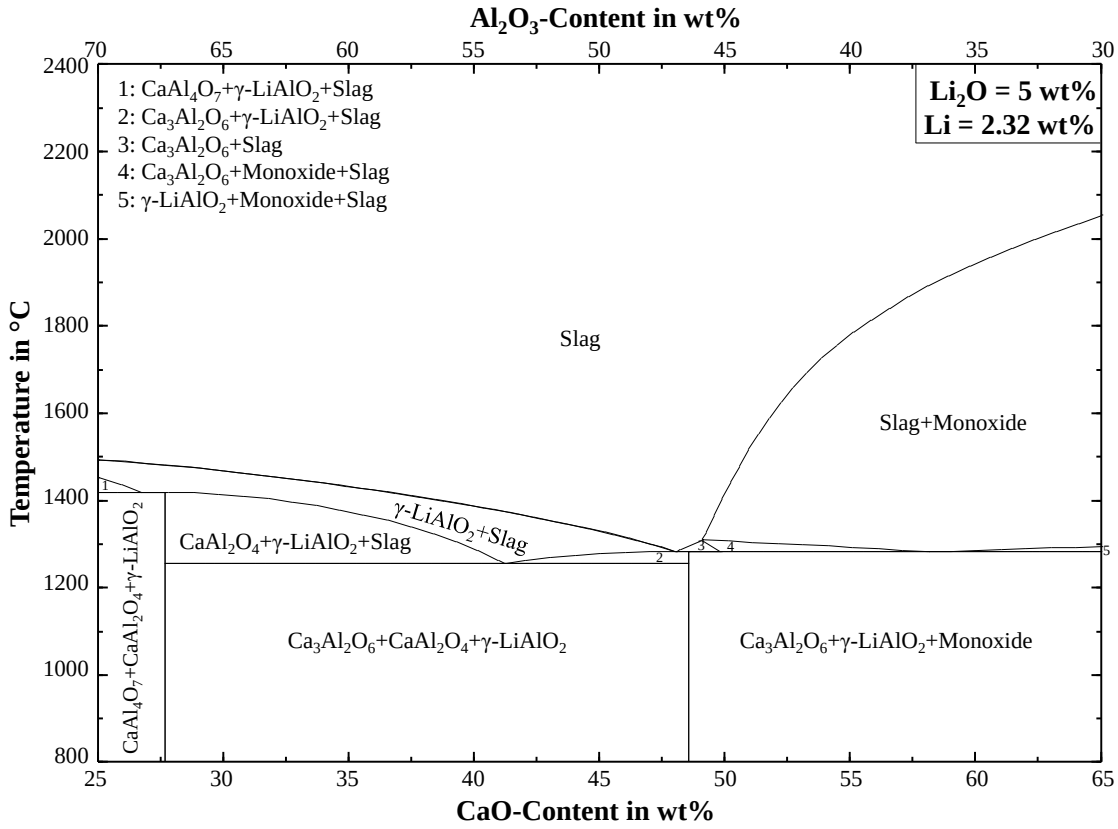

Figure 9: CaO-Al_2O_3 Phase Diagram with a constant Li_2O-content of 5 wt%

A Li_2O-content of around 5 wt% is only achieved in the trials with a lime addition of 13 wt% and a smelting temperature of 1800 °C. The mean and normalized Al_2O_3-content is 38.3 wt% and the CaO-content is 55.3 wt%. Therefore, according to the phase diagram, the first phase field where the slag is fully solidified is the $Ca_3Al_2O_6$+γ-$LiAlO_2$+Monoxide(CaO) field.

Figure 10 shows the Al_2O_3-CaO phase diagram with a constant Li_2O-content of 10 wt%.

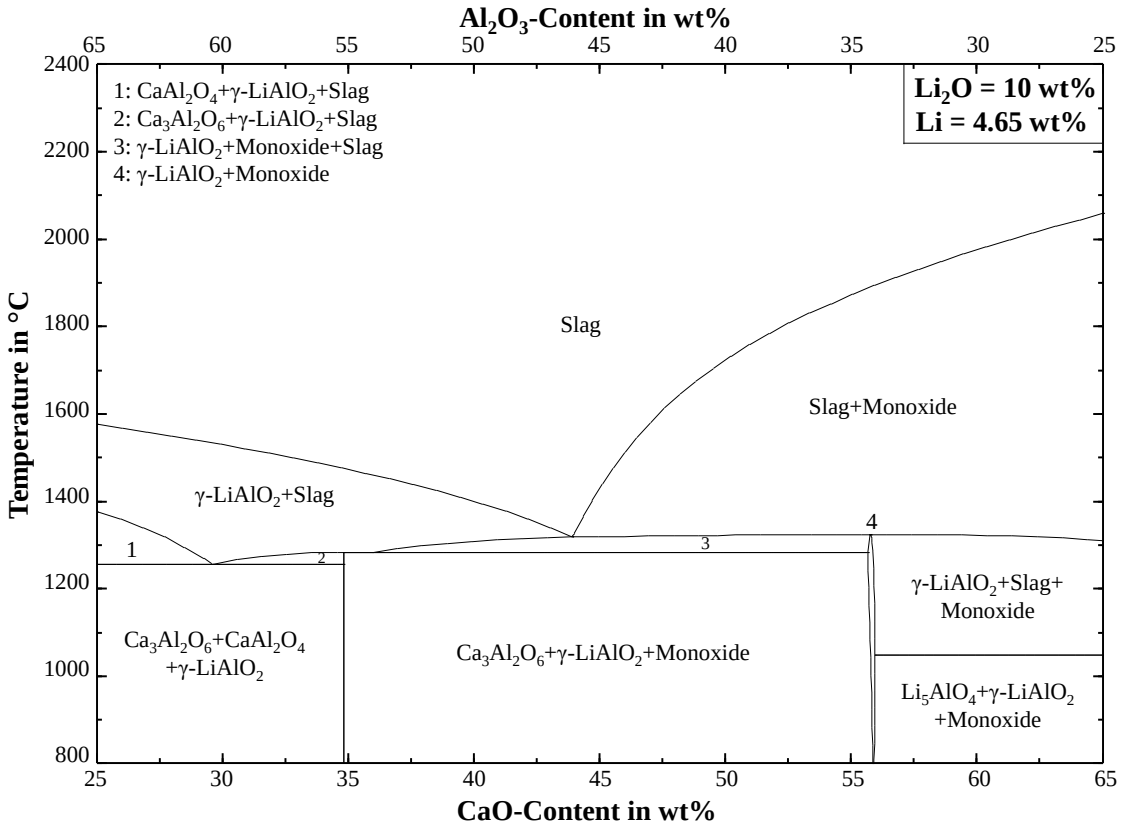

Figure 10: CaO-Al_2O_3 Phase Diagram with a constant Li_2O-content of 10 wt%

The trials at 1800 °C with a lime addition of 10 wt% and the trials at 1700 °C with a lime addition of 13 wt% are comparable to this phase diagram. Even though the ratio of CaO to Al_2O_3 in the slags is deviating according to Table 11, the first phase field where the slags from both parameter combinations are fully solidified is the $Ca_3Al_2O_6$+γ-$LiAlO_2$+Monoxide(CaO) field.

Figure 11 shows the Al_2O_3-CaO phase diagram with a constant Li_2O-content of 15 wt%.

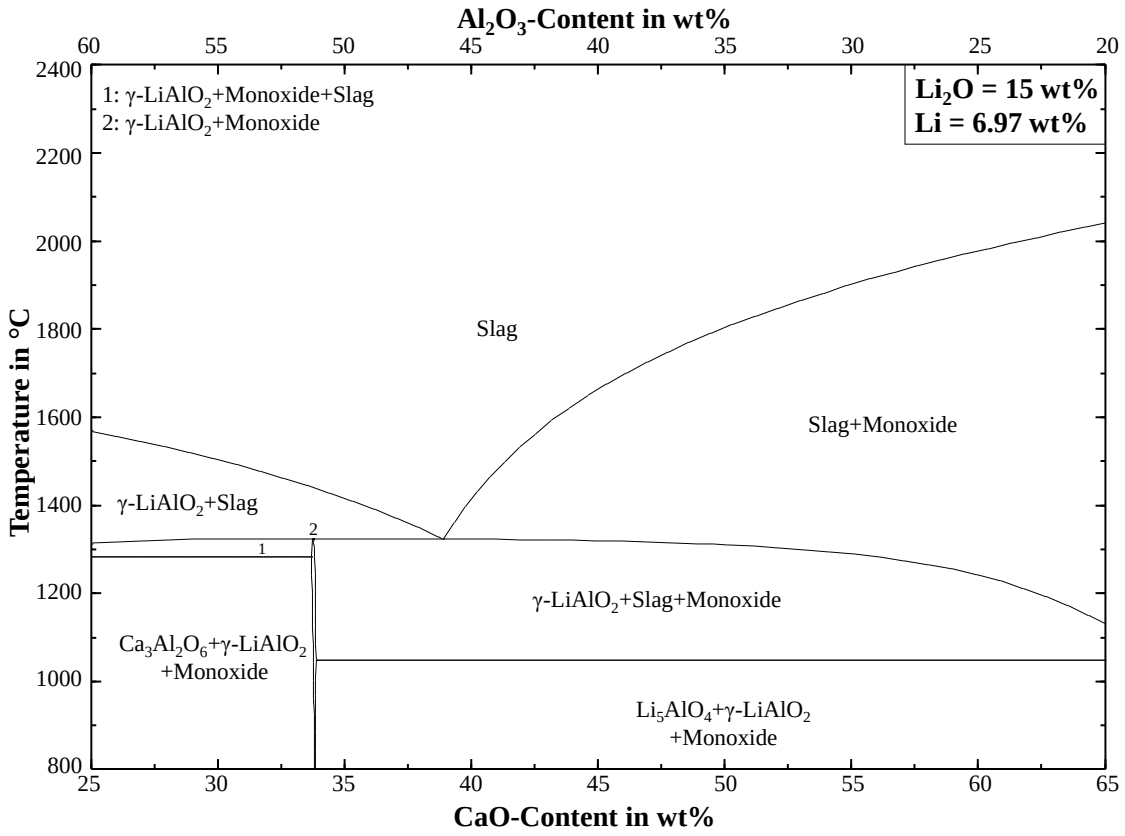

Figure 11: $CaO\text{-}Al_2O_3$ Phase Diagram with a constant Li_2O-content of 15 wt%

The trials at 1800 °C with a lime addition of 7 wt% and the trials at 1700 °C with a lime addition of 7 wt% and 10 wt% are comparable to this phase diagram. Compared to the phase diagrams with a lower lithium content, this time the first phase field where the slags from the three parameter combinations are fully solidified is the Li_5AlO_4+γ-$LiAlO_2$+Monoxide(CaO) field. According to the phase diagram, no calcium aluminates would form, because the mean and normalized CaO-content in the samples relevant for this phase diagram is above 41.0 wt%.

4.2 X-Ray Diffraction Analysis of Slag Samples

An X-ray diffraction (XRD) powder spectrometer with a copper anode (40 kV, 30 mA) was used to analyze slag samples. The spectrometer was equipped with a Germanium monochromator to use the Kα1-radiation with a wavelength of 1.540598 Å. Reference data from the "Crystallography Open Database" was used for the evaluation.

Figure 12 shows the XRD-pattern of the slags generated in the experimental work. The slags are sorted by descending lithium contents.

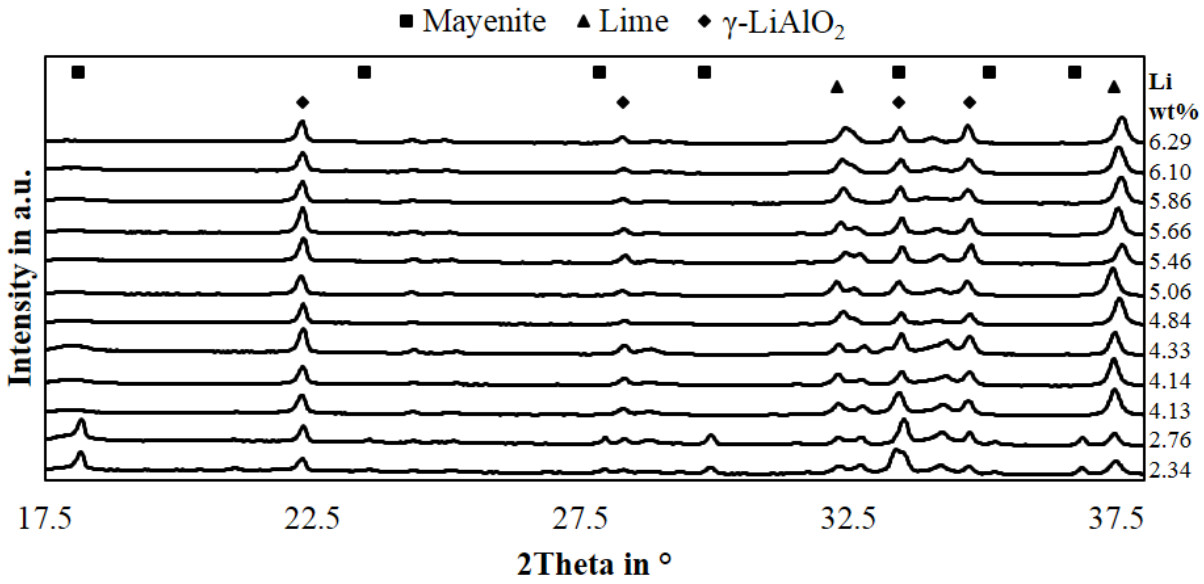

Figure 12: XRD-Pattern of slag samples sorted by lithium content

Comparing the results with the phase diagrams, the presence of lime and γ-$LiAlO_2$ is predicted by the simplified phase diagram for every relevant composition, this is also confirmed by the XRD-analysis. However, the lime is not stable and resulted in a slag decay after several months of storage. The presence of tricalcium aluminate was predicted by the phase diagrams for Li_2O-contents of 5 wt% and 10 wt% but could not be confirmed by XRD. Instead, for trials at 1800 °C and a lime addition of 13 wt%, the presence of Mayenite ($Ca_{12}Al_{14}O_{32}$) was observed by XRD, another explanation for the peaks could be $Ca_{12}Al_{14}O_{32}F_2$, which has peaks at the same position as Mayenite. The presence of Li_5AlO_4 predicted in the phase diagram for Li_2O-contents of 15 wt% could also not be confirmed by XRD.

However, a few unresolved questions remain after the XRD-analysis, there is no explanation for the appearing peak at a 2Theta value of 32.7° for decreasing lithium contents and the peak at 34.15° could not be explained by the shown minerals in the figure.

5 Conclusion

The smelting of pyrolyzed lithium-ion black mass yielded a slag with low copper, nickel and cobalt contents. The lithium content in the slag can still be considered quite high with up to 6.2 wt% of lithium, even though less lithium is transferred to the slag compared to the amount of lithium in the raw material and therefore an accumulation of lithium in the flue dust is the result.

Based on the results, a complete volatilization of lithium in the smelting process seems to be difficult. The best results were achieved adding 13 wt% lime at a temperature of 1800 °C, however, still 16.80 % of lithium was transferred to the slag phase and assuming that 2.8 % of lithium is transferred to the metal phase as it was reported in an earlier study with the same raw material [22], 19.6 % of lithium would be lost in total in the slag and metal phase while 80.4 % of lithium would be enriched

in the flue dust. In this case, the lithium content in the slag is still 2.34 wt% mostly in the form of γ-$LiAlO_2$. As this content of lithium is relatively low, it is doubtful, if lithium can be recovered economically from the produced slag. To increase the volatilization of lithium, higher temperatures or longer holding times could be an option, but this would increase the energy consumption, especially because the process temperature of 1800 °C is already relatively high. The addition of elements, which form lithium compounds with a higher vapor pressure could be another option. Halides could be suitable, but this would also result in higher wear in the off-gas system or for the refractory lining of the furnace. Furthermore, adjusting the composition of the charged material could be helpful, since lithium remains in the slag as γ-$LiAlO_2$ and the addition of aluminum oxide increases the lithium slagging according to a FactSage™ simulation compiled in a previous study [22], a lower aluminum content in the input material should increase the volatilization efficiency. This would mean, that for higher volatilization the separation processes before the smelting operation have to remove more aluminum from the raw material. Another problem to overcome is the simultaneous recovery of lithium and valuable metals like cobalt from the flue dust. Since Georgi-Maschler et.al. [24] reported elevated cobalt contents in the flue dust, a hydrometallurgical process to treat the flue dust cannot only focus on the lithium recovery, but has to recover cobalt as well. Especially considering the slightly higher cobalt prices compared to the lithium prices. Table 5 shows an estimate of the value of flue dust gathered by Georgi-Maschler et.al. [24], using the mean commodity price for cobalt and lithium carbonate between October 2019 and September 2020 [48] and the exchange rate from RMB to US$ valid on the 28th October 2020. Costs for extraction and refining are neglected in this calculation and it is assumed, that the recovered products are pure enough to be sold without a discount.

Table 5: Economic value of metals in flue

Commodity	Price per Ton [48]	Composition of Flue Dust [24]	Value of the extracted Metal per ton of Dust
Co	37,655.79 US$/t	19.4 wt%	7305 US$
Li_2CO_3	45,579.67 RMB/t	-	-
Li (as Li_2CO_3)	36,049.07 US$/t	20.1 wt%	7246 US$

Even though the lithium content in the flue dust sample is higher than the cobalt content [24], the value of cobalt is higher in the dust. Based on the used price per ton, the lithium content in the dust needs to be 4.46 % higher in relation to the cobalt content to hit the break-even point where the mass of lithium is more valuable than the mass of cobalt in the flue dust.

However, in a pilot-scale study carried out by Hu et.al. [39] lower cobalt concentrations and also nickel concentrations in the flue dust were reported. In two trials, average lithium contents of 12.40 wt% and 13.02 wt% were reported. The average cobalt concentrations were 1.46 wt% and 0.97 wt% and the average nickel concentrations were 4.32 wt% and 2.17 wt%. Reported lithium yields in the flue dust were 68.3 wt% and 60.9 wt% [39]. In this case, the lithium would be more

valuable than the cobalt in the flue dust, even though the lithium yield during smelting is still quite low.

6 Recommendations for a Process with a High Lithium Yield

Due to the reported cobalt contents in the flue dust, the high smelting temperatures needed to volatilize a major share of lithium, and the lithium losses into the slag, a smelting process aiming to volatilize lithium may not be suitable. Another obstacle to overcome is the high carbon content present in black mass, since smelting of the black mass without the addition of copper(II)-oxide yielded a mushy slag and graphite mixture with a high viscosity. As shown in this work and in our previous study [22], graphite can be used as a reducing agent for added metal oxides, but the addition of pure metal oxides to use graphite from battery scrap as a reducing agent is probably not an option for an industrial process. A more technical viable approach proposed by Ruismäki et.al. [18, 29] and Avarmaa et.al [49] is the usage of battery scrap as a reductant for nickel slag cleaning operations, probably battery scrap would work for other kinds of oxidic raw materials containing cobalt, nickel or copper, but a high dilution of lithium in the slag could be expected then, which would result in a slag with low lithium contents not suitable for economic lithium extraction. Furthermore, the dilution of lithium in the slag can inhibit the enrichment of lithium in the flue dust, since the dilution of lithium in the slag may decrease the volatilization.

A possible flowsheet to overcome the problem of the high graphite content could be a graphite separation before smelting of battery scrap like black mass. One option for this could be flotation, which was already investigated by several researchers [13, 18, 50–53]. As a significant portion of lithium seems to be always lost in the slag, an enrichment of lithium in slag instead of the flue dust might be beneficial. Fluxes like SiO_2 or Al_2O_3 could then be an option to promote the slagging of lithium as investigated earlier [22]. Valuable metals like cobalt, nickel and copper are then enriched in a metal alloy. The slag rich in lithium could be used as an artificial ore to recover the lithium, for example using a dry digestion process with sulfuric acid as studied by Klimko et.al. [43]. By returning the flue dust into the smelting furnace, the yields for cobalt, nickel and copper in the alloy could be increased and also the yield for lithium in the slag could be increased, the lithium losses during smelting would be reduced to the portion of lithium, that is transferred to the alloy. However, enrichment of other elements that are volatilized during smelting could be a problem, if the flue dust is permanently recycled back to the smelting furnace. A pre-treatment of the dust could be necessary, to remove elements like halides, which are easily volatilized and can decrease the lifetime of the off-gas system [27, 54–56]. The flowsheet containing the described unit operations is shown in Figure 13.

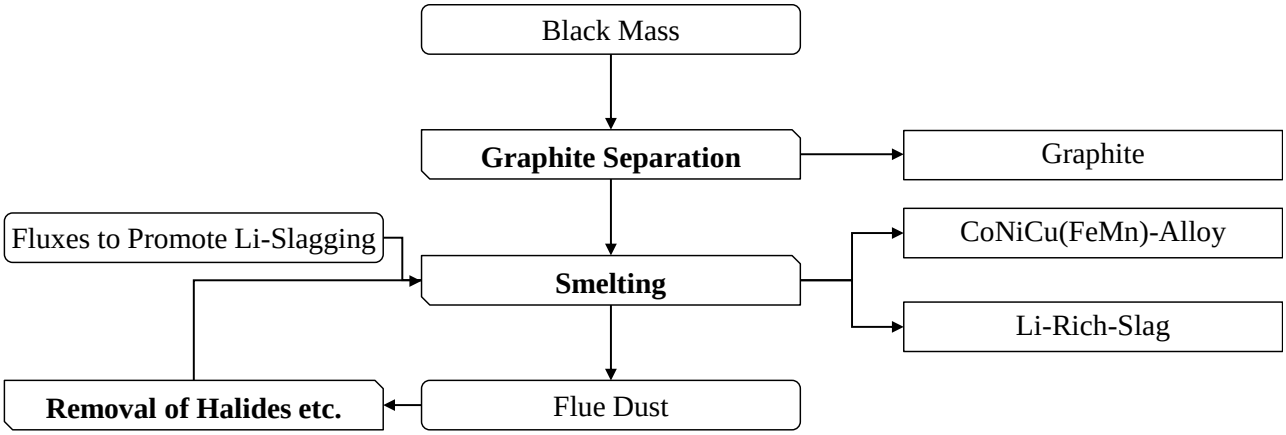

Figure 13: Proposed Flowsheet for a multi-metal recovery

As some studies were already carried out investigating the pyrometallurgical treatment of battery scrap, those results can be compared to highlight advantages and disadvantages of the enrichment of lithium in the slag or flue dust. Table 6 summarizes some relevant categories based on the results by three different authors investigating the smelting of lithium battery scrap in electric arc furnaces.

Table 6: Advantages and Disadvantages of Li-Slagging and Li-Volatilization

Category	**This Study**	**Previous Study [22]**	**Georgi-Maschler et.al. [24]**	**Hu et.al. [39]**
Li-Yield	80.4 %	82.4 %	68.6 %	68.3 % & 60.9 %
Li-Content in Intermediate Product	Not Determined (Flue Dust)	7.4 wt% (Slag)	20.1 wt% (Flue Dust)	12.4 wt% & 13.02 wt% (Flue Dust)
Process Temperature	1800 °C	1600 °C	1750 °C	1600 °C
Investigated Scale	Laboratory	Laboratory	Technical	Pilot

The lithium yield in the flue dust obtained in this study surpasses the previous results obtained by Georgie-Maschler et.al [24] and Hu et.al. [39], even though a comparison is limited by different raw materials used in the studies and different scales. Furthermore, the current study used the highest process temperature, which is a clear disadvantage, especially compared to the work carried out by Hu et.al. [39]. One more advantage of the studies by Georgie-Maschler et.al [24] and Hu et.al. [39] is the high lithium content in the flue dust, which surpasses the lithium content in the slag obtained in our previous study [22]. The flue dust in this stury was not sampled due to technical reasons and the lithium content can not be presented in this work. However, the lithium losses of 16.80 % into the slag reported in the current study are a problem if enrichment of lithium in the flue dust is aimed for, as a recovery of lithium from slag and flue dust generated in the same smelting process might be too costly. Therefore, the lithium present in the slag would be lost.

As the enrichment of lithium in the slag or the flue dust is both accompanied by advantages and disadvantages considering the process or the quality of the intermediate product, it is difficult to state the superior process and more work has to be carried out to investigate the whole process chain, since most authors only focused on one option to recycle battery waste or only on one process step.

References

[1] Dańczak, A., Klemettinen, L., Kurhila, M., Taskinen, P., Lindberg, D. and Jokilaakso, A. (2020) Behavior of Battery Metals Lithium, Cobalt, Manganese and Lanthanum in Black Copper Smelting. Batteries, 6, 1, 16.

[2] Helbig, C., Bradshaw, A.M., Wietschel, L., Thorenz, A. and Tuma, A. (2018) Supply risks associated with lithium-ion battery materials. Journal of Cleaner Production, 172, 274–286.

[3] Nitta, N., Wu, F., Lee, J.T. and Yushin, G. (2015) Li-ion battery materials: present and future. Materials Today, 18, 5, 252–264.

[4] Gu, F., Guo, J., Yao, X., Summers, P.A., Widijatmoko, S.D. and Hall, P. (2017) An investigation of the current status of recycling spent lithium-ion batteries from consumer electronics in China. Journal of Cleaner Production, 161, 765–780.

[5] Contestabile, M., Panero, S. and Scrosati, B. (2001) A laboratory-scale lithium-ion battery recycling process. Journal of Power Sources, 92, 1–2 65–69.

[6] Pinegar, H. and Smith, Y.R. (2020) Recycling of End-of-Life Lithium-Ion Batteries, Part II: Laboratory-Scale Research Developments in Mechanical, Thermal, and Leaching Treatments. Journal of Sustainable Metallurgy, 6, 142–160.

[7] Porvali, A. et al. (2019) Mechanical and hydrometallurgical processes in HCl media for the recycling of valuable metals from Li-ion battery waste. Resources, Conservation and Recycling, 142, 257–266.

[8] Pinegar, H. and Smith, Y.R. (2019) Recycling of End-of-Life Lithium Ion Batteries, Part I: Commercial Processes. Journal of Sustainable Metallurgy, 5, 402–416.

[9] Tarascon, J. and Armand, M. (2001) Issues and challenges facing rechargeable lithium batteries. Nature, 414, 359–367.

[10] Huang, B., Pan, Z., Su, X. and An, L. (2018) Recycling of lithium-ion batteries: Recent advances and perspectives. Journal of Power Sources, 399, 274–286.

[11] Werner, D., Peuker, U.A. and Mütze, T. (2020) Recycling Chain for Spent Lithium-Ion Batteries. Metals, 10, 3, 316.

[12] Zhong, X., Liu, W., Han, J., Jiao, F., Qin, W. and Liu, T. (2020) Pretreatment for the recovery of spent lithium ion batteries: theoretical and practical aspects. Journal of Cleaner Production, 263, 121439.

[13] Liu, J. et al. (2020) Recovery of LiCoO2 and graphite from spent lithium-ion batteries by cryogenic grinding and froth flotation. Minerals Engineering, 148, 106223.

[14] Zhang, G., Du, Z., He, Y., Wang, H., Xie, W. and Zhang, T. (2019) A Sustainable Process for the Recovery of Anode and Cathode Materials Derived from Spent Lithium-Ion Batteries. Sustainability, 11, 8, 2363.

[15] Zhang, G., He, Y., Feng, Y., Wang, H., Zhang, T., Xie, W. and Zhu, X. (2018) Enhancement in liberation of electrode materials derived from spent lithium-ion battery by pyrolysis. Journal of Cleaner Production, 199, 62–68.

[16] Li, J., Lai, Y., Zhu, X., Liao, Q., Xia, A., Huang, Y. and Zhu, X. (2020) Pyrolysis kinetics and reaction mechanism of the electrode materials during the spent LiCoO2 batteries recovery process. Journal of Hazardous Materials, 398, 122955.

[17] Zhong, X., Liu, W., Han, J., Jiao, F., Qin, W., Liu, T. and Zhao, C. (2019) Pyrolysis and physical separation for the recovery of spent LiFePO4 batteries. Waste Management, 89, 83–93.

[18] Ruismäki, R., Rinne, T., Dańczak, A., Taskinen, P., Serna-Guerrero, R. and Jokilaakso, A. (2020) Integrating Flotation and Pyrometallurgy for Recovering Graphite and Valuable Metals from Battery Scrap. Metals, 10, 5, 680.

[19] Shi, J. et al. (2019) Sulfation Roasting Mechanism for Spent Lithium-Ion Battery Metal Oxides Under SO2-O2-Ar Atmosphere. JOM, 71, 4473–4482.

[20] Peng, C., Hamuyuni, J., Wilson, B.P. and Lundström, M. (2018) Selective reductive leaching of cobalt and lithium from industrially crushed waste Li-ion batteries in sulfuric acid system. Waste Management, 76, 582–590.

[21] Porvali, A., Chernyaev, A., Shukla, S. and Lundström, M. (2020) Lithium ion battery active material dissolution kinetics in Fe(II)/Fe(III) catalyzed Cu-H2SO4 leaching system. Separation and Purification Technology, 236, 116305.

[22] Sommerfeld, M. et al. (2020) A Combined Pyro- and Hydrometallurgical Approach to Recycle Pyrolyzed Lithium-Ion Battery Black Mass Part 1: Production of Lithium Concentrates in an Electric Arc Furnace. Metals, 10, 8, 1069.

[23] Harper, G. et al. (2019) Recycling lithium-ion batteries from electric vehicles. Nature 575, 75–86.

[24] Georgi-Maschler, T., Friedrich, B., Weyhe, R., Heegn, H. and Rutz, M. (2012) Development of a recycling process for Li-ion batteries. Journal of Power Sources, 207, 173–182.

[25] Wang, H. and Friedrich, B. (2015) Development of a Highly Efficient Hydrometallurgical Recycling Process for Automotive Li–Ion Batteries. Journal of Sustainable Metallurgy, 1, 168–178.

[26] Vest, M., Georgi-Maschler, T., Friedrich, B. and Weyhe, R. (2010) Rückgewinnung von Wertmetallen aus Batterieschrott. Chemie Ingenieur Technik, 82, 11, 1985–1990.

[27] Murakami, Y., Matsuzaki, Y., Murakami, K., Hiratani, S., Shibayama, A. and Inoue, R. (2020) Recovery Rates of Used Rechargeable Lithium-Ion Battery Constituent Elements in Heat Treatment. Metallurgical and Materials Transactions B, 51, 135–1362.

[28] Marshall, J., Gastol, D., Sommerville, R., Middleton, B., Goodship, V. and Kendrick, E. (2020) Disassembly of Li Ion Cells—Characterization and Safety Considerations of a Recycling Scheme. Metals, 10, 6, 773.

[29] Ruismäki, R., Dańczak, A., Klemettinen, L., Taskinen, P., Lindberg, D. and Jokilaakso, A. (2020) Integrated Battery Scrap Recycling and Nickel Slag Cleaning with Methane Reduction. Minerals, 10, 5, 435.

[30] Brückner, L., Frank, J. and Elwert, T. (2020) Industrial Recycling of Lithium-Ion Batteries—A Critical Review of Metallurgical Process Routes. Metals, 10, 8, 1107.

[31] Sabarny, P., Peters, L., Sommerfeld, M., Stallmeister, C., Schier, C. and Friedrich, B. (2020) Early-Stage Lithium Recovery (ESLR) for Enhancing Efficiency in Battery Recycling. AABC Europe 2020: Advanced Automotive Battery Conference.

[32] He, S., Wilson, B.P., Lundström, M. and Liu, Z. (2020) Clean and efficient recovery of spent LiCoO2 cathode material: Water-leaching characteristics and low-temperature ammonium sulfate calcination mechanisms. Journal of Cleaner Production, 268, 122299.

[33] Peng, C. et al. (2020) Role of impurity copper in Li-ion battery recycling to LiCoO2 cathode materials. Journal of Power Sources, 450, 227630.

[34] Ren, G.X., Xiao, S.W., Xie, M.Q., Pan, B., Chen, J., Wang, F.G. and Xia, X. (2017) Recovery of valuable metals from spent lithium ion batteries by smelting reduction process based on FeO–SiO2–Al2O3 slag system. Transactions of Nonferrous Metals Society of China, 27, 2, 450–456.

[35] Xiao, S., Ren, G., Xie, M., PAN, B., Fan, Y., Wang, F. and Xia, X. (2017) Recovery of Valuable Metals from Spent Lithium-Ion Batteries by Smelting Reduction Process Based on MnO–SiO2–Al2O3 Slag System. Journal of Sustainable Metallurgy, 3, 703–710.

[36] Hu, X., Mousa, E., Tian, Y. and Ye, G. (2020) Recovery of Co, Ni, Mn, and Li from Li-ion batteries by smelting reduction - Part I: A laboratory-scale study. Journal of Power Sources, 483, 228936.

[37] Guoxing, R., Songwen, X., Meiqiu, X., Bing, P., Youqi, F., Fenggang, W. and Xing, X. (2016) Recovery of Valuable Metals from Spent Lithium-Ion Batteries by Smelting Reduction Process Based on MnO-SiO2-Al2O3 Slag System. Proceedings of the 10th International Conference on Molten Slags, Fluxes, and Salts, 211–218.

[38] M Vest, J Zervos, R Weyhe and B Friedrich (2010) Slag Design for Lithium Recovery from Spent Batteries. International Workshop on Metal-Slag Interaction, Yalta Ukraine.

[39] Hu, X., Mousa, E. and Ye, G. (2021) Recovery of Co, Ni, Mn, and Li from Li-ion batteries by smelting reduction - Part II: A pilot-scale demonstration. Journal of Power Sources, 483, 229089.

[40] Dang, H. et al. (2020) Lithium leaching via calcium chloride roasting from simulated pyrometallurgical slag of spent lithium ion battery. Separation and Purification Technology, 233, 116025.

[41] Dang, H. et al. (2018) Recycled Lithium from Simulated Pyrometallurgical Slag by Chlorination Roasting. ACS Sustainable Chemistry and Engineering, 6, 10, 13160–13167.

[42] Li, N. et al. (2019) Aqueous leaching of lithium from simulated pyrometallurgical slag by sodium sulfate roasting. RSC Advances, 9, 23908–23915.

[43] Klimko, J. et al. (2020) A Combined Pyro- and Hydrometallurgical Approach to Recycle Pyrolyzed Lithium-Ion Battery Black Mass Part 2: Lithium Recovery from Li Enriched Slag—Thermodynamic Study, Kinetic Study, and Dry Digestion. Metals, 10, 11, 1558.

[44] Bale, C.W. et al. (2016) FactSage Thermochemical Software and Databases - 2010 – 2016. Calphad, 54, 35–53.

[45] Kallitsis, E., Korre, A., Kelsall, G., Kupfersberger, M. and Nie, Z. (2020) Environmental life cycle assessment of the production in China of lithium-ion batteries with nickel-cobalt-manganese cathodes utilising novel electrode chemistries. Journal of Cleaner Production, 254, 120067.

[46] Plewa, J. and Skrzypek, J. (1989) Kinetics of the reduction of copper oxide with carbon monoxide. Chemical Engineering Science, 44, 12, 2817–2824.

[47] Keber, S., Brückner, L., Elwert, T. and Kuhn, T. (2020) Concept for a Hydrometallurgical Processing of a Copper-Cobalt-Nickel Alloy Made from Manganese Nodules. Chemie Ingenieur Technik, 92, 4, 379–386.

[48] Deutsche Rohstoffagentur (2020) Preismonitor September 2020.

[49] Avarmaa, K., Järvenpää, M., Klemettinen, L., Marjakoski, M., Taskinen, P., Lindberg, D. and Jokilaakso, A. (2020) Battery Scrap and Biochar Utilization for Improved Metal Recoveries in Nickel Slag Cleaning Conditions. Batteries, 6, 4, 58.

[50] He, Y., Zhang, T., Wang, F., Zhang, G., Zhang, W. and Wang, J. (2017) Recovery of LiCoO2 and graphite from spent lithium-ion batteries by Fenton reagent-assisted flotation. Journal of Cleaner Production, 143, 319–325.

[51] Yu, J., He, Y., Ge, Z., Li, H., Xie, W. and Wang, S. (2018) A promising physical method for recovery of LiCoO 2 and graphite from spent lithium-ion batteries: Grinding flotation. Separation and Purification Technology, 190, 45–52.

[52] Zhang, G., He, Y., Feng, Y., Wang, H. and Zhu, X. (2018) Pyrolysis-Ultrasonic-Assisted Flotation Technology for Recovering Graphite and LiCoO 2 from Spent Lithium-Ion Batteries. ACS Sustainable Chemisty and Engineering, 6, 8, 10896–10904.

[53] Zhang, G., He, Y., Wang, H., Feng, Y., Xie, W. and Zhu, X. (2019) Application of mechanical crushing combined with pyrolysis-enhanced flotation technology to recover graphite and LiCoO2 from spent lithium-ion batteries. Journal of Cleaner Production, 231, 1418–1427.

[54] Grudinsky, P.I., Dyubanov, V.G. and Kozlov, P.A. (2019) Copper Smelter Dust Is a Promising Material for the Recovery of Nonferrous Metals by the Waelz Process. Inorganic Materials: Applied Research, 10, 496–501.

[55] Halli, P., Hamuyuni, J., Revitzer, H. and Lundström, M. (2017) Selection of leaching media for metal dissolution from electric arc furnace dust. Journal of Cleaner Production, 164, 265–276.

[56] Aromaa, J., Kekki, A., Stefanova, A., Makkonen, H. and Forsén, O. (2016) New hydrometallurgical approaches for stainless steel dust treatment. Mineral Processing and Extractive Metallurgy, 125, 4, 242–252.